Astron. Astrophys. 325, 664–676 (1997)

ASTRONOMY
AND
ASTROPHYSICS

The X-ray coronal emission of λ Andromedae observed with ASCA and ROSAT

A. Ortolani[1], **A. Maggio**[2], **R. Pallavicini**[2], **S. Sciortino**[2], **J.J. Drake**[3], **and S.A. Drake**[4]

[1] Osservatorio Astrofisico di Arcetri, Largo Fermi 5, I-50125 Firenze, Italy
[2] Osservatorio Astronomico di Palermo, Piazza del Parlamento 1, I-90134 Palermo, Italy
[3] Center for Astrophysics, 60 Garden St., Cambridge, MA 02138, USA
[4] NASA Goddard Space Flight Center, Greenbelt, MD 20771, USA

Received 7 January 1997 / Accepted 24 March 1997

Abstract. We present an observation of the long-period RS CVn binary λ And obtained with ASCA. We also discuss a previous observation by ROSAT of the same star, that we have retrieved from the public archive. There was little variation in the quiescent X-ray flux of λ And between these two observations almost 5 years apart, but they offer different, and in part complementary, views of its corona. The ASCA spectra of λ And are well described by a 2-T model with a main component at $T_1 \simeq 0.9$ keV and a smaller component at $T_2 \simeq 3$ keV, with $EM_2/EM_1 \simeq 0.15$. The fitted coronal metallicity is $Z \simeq 0.1$, much lower than solar but consistent within a factor of 2 with the reported photospheric metallicity $Z_{phot} \simeq 0.2$. On the contrary, a successful 2-T fit of the ROSAT spectrum yields a cool component at $\simeq 0.5$ keV and a hotter component at $\simeq 1.4$ keV, with $EM_2/EM_1 \simeq 2$ and $Z \simeq 0.25$. Because of these differences, we were unable to find an acceptable fit to the joint ASCA and ROSAT data. We discuss possible causes for the discrepancy, including spectral time variability, uncertainties in the plasma emission codes and in the instrumental calibration, and limitations in the adopted fitting model. The hydrogen column density toward λ And, well constrained by ROSAT, is $N_{\rm H} \simeq 1 \times 10^{19}$ cm^{-2}, a factor ~ 2 larger than estimated from UV observations from Copernicus and the Hubble Space Telescope. Albeit small, this difference may indicate the presence of substantial ionization of the interstellar medium.

Key words: stars: coronae – stars: late-type – stars: abundances – stars: individual: λ And – X-rays: stars

1. Introduction

RS CVn binaries are among the strongest late-type coronal X-ray sources and for this reason they have been natural targets for spectroscopic observations at X-ray and UV wavelengths with IUE, *Einstein*, EXOSAT and, more recently, ROSAT, EUVE and ASCA (Swank et al. 1981; Majer et al. 1986; Pasquini et al. 1989; Culhane et al. 1990; White et al. 1990, 1994; Dempsey et al. 1993a,b; Drake et al. 1994; Ortolani et al. 1997). Defined as a class by Hall (1976), RS CVn's typically consist of a G or K-type giant or subgiant with a late-type main-sequence or subgiant companion. Orbital periods range from order of one day to several tens of days. Tidal interaction between the two components is thought to spin up the stars such that the RS CVn's with orbital periods shorter than about 30 days have rotation periods synchronized with the system orbital periods (e.g. Habets & Zwaan 1989). Fast rotation, and also perhaps tidal interaction itself (e.g. Schrijver & Zwaan 1991), is then believed to stimulate magnetic dynamo action which must, ultimately, be responsible for the observed surface activity.

Several RS CVn binaries have been studied spectroscopically at X-ray and EUV wavelengths with ASCA and EUVE. These studies have uncovered an unexpected puzzle: both ASCA and EUVE spectra of RS CVn's, and also of Algol binaries and active single stars, appear to be indicating that their coronae are significantly metal deficient with respect to the Sun—by factors of 3 to as much as 10 (White et al. 1994; Antunes et al. 1994; Drake et al. 1994; Gotthelf et al. 1994; Singh et al. 1995, 1996; Stern et al. 1995; Schmitt et al. 1996a,b; Schrijver et al. 1995; Mewe et al. 1996, Tagliaferri et al. 1996). Alternative physical explanations have been sought for the apparent metal deficiencies, such as resonant scattering of emission line photons (e.g. Schrijver et al. 1994, 1995; Mewe et al. 1995). However, others have argued against this picture (e.g. Schmitt et al. 1996a), and metal deficiency remains the most plausible scenario for both the EUVE and ASCA results.

The coronal results are perhaps not unexpected when considered in the light of the rather sparse photospheric abundance studies of these very active stars. Hints from optical work that RS CVn's might be metal poor in their photospheres relative to the Sun came from earlier work (e.g. Naftilan & Drake 1977, 1980; Fekel et al. 1987), and were confirmed by later studies (e.g. Randich et al. 1993, 1994). The problem however is that

Send offprint requests to: A. Maggio

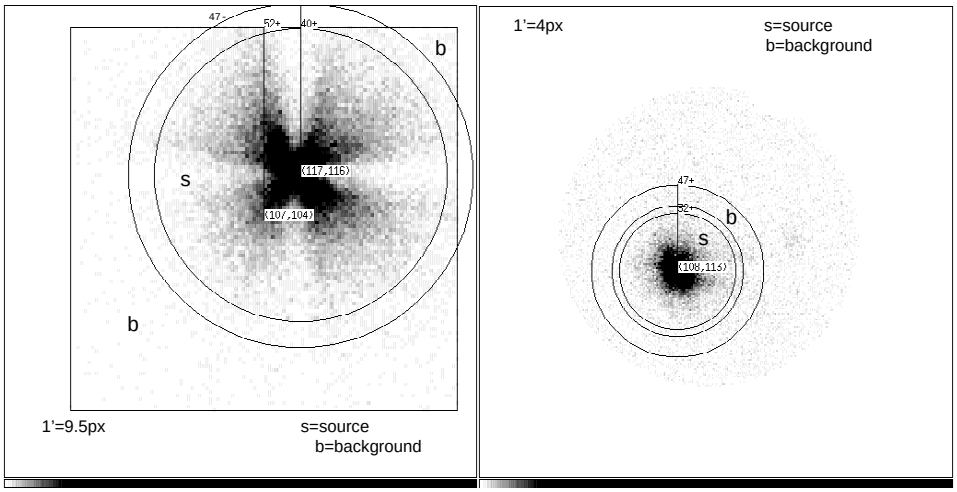

Fig. 1. *ASCA* SIS0 (to the left) and GIS2 (to the right) images of λ And. The photon collecting regions for source and background are indicated

the Algols, RS CVn's and active stars are thought to be relatively young and are not, on the whole, expected to be metal poor. Based on their estimated ages—about 2-3 Gyr for the RS CVn's (e.g. Eker 1992 and references therein) and < 1 Gyr for the Algol binaries—the age-metallicity relation for the solar vicinity (e.g. Edvardsson et al. 1993) implies that these stars should have a mean [Fe/H]= -0.1 or so, with scatter between +0.3 and -0.4. At face value, the RS CVn's and Algols do not fit this picture, and this led several authors (e.g. Fekel et al. 1987, Randich et al. 1993) to suggest that the photospheric lines must be filled in by chromospheric activity, causing only an apparent metal deficiency. [1]. While this might be the case with the photospheric absorption lines, this argument still leaves their coronae apparently metal poor and unexplained.

In this paper we examine the ASCA spectrum of the long-period RS CVn λ And in order to probe its coronal composition and compare these findings with earlier results concerning its photospheric composition. This system consists of a G8 III-IV primary with a rotation period of 54 days and an unseen companion in an orbit with a period of 20.5 days (Strassmeier et al. 1989); the system is therefore asynchronous. λ And is one of the brightest long-period RS CVn's at X-ray wavelengths. In the absence of any firm clues as to the identity of the secondary, the primary component is thought to be wholly responsible for the observed X-ray emission—an appealing quality which offers the simplifying advantage that the secondary star needs not be considered in the interpretation of the X-ray spectrum. Similarly, the non-detection of the secondary companion offers the same advantage with regard to its photospheric spectrum at optical wavelengths. Indeed, unlike the RS CVn's with composite spectra, the photospheric metallicity of λ And appears to be reasonably well-constrained at about [Fe/H]=-0.7 (i.e. $\simeq$ 0.2 solar; Anders & Grevesse 1989), with a scatter about this value of 0.15 dex or so from the different studies published to-date (Helfer & Wallerstein 1968, Taylor 1991, Tautvaisiene et al. 1992, Savanov & Berdyugina 1994, Randich et al. 1994). λ And was observed previously with *Einstein* and EXOSAT (Swank et al. 1981; Mayer et al. 1986; Mewe & Schrijver 1987; Ortolani et al. 1997) but those early data could not provide any stringent constraint on coronal metallicity (i.e. it was consistent with solar).

This paper is organized as follows. In Sect. 2 we first describe the ASCA data obtained in our Guest Investigator program (co-PI's: J. Drake and R. Pallavicini). Then, in Sect. 3, we discuss earlier ROSAT data that we have retrieved from the ROSAT public archive. Our results are discussed in Sect. 4.

2. The ASCA data

2.1. Observations and data reduction

λ And was observed by ASCA on January 6-7, 1996 from 22:17 to 19:06 UT. The data were acquired with the two Solid State Imaging Spectrometers (SIS0 and SIS1) in the 1-CCD mode, and with the two Gas Imaging Spectrometers (GIS2 and GIS3). For a detailed description of the ASCA instrumentation see Tanaka et al. (1994).

For both the SIS and GIS data we adopted the standard screening criteria recommended by the ASCA team (Day et al. 1995), which resulted in a useful exposure time of about 30 ksec. We accumulated the counts and the pulse height spectra from a circular region which possibly contained 98% of the total energy at 1 keV. This gave for the GIS a region of about 8 arcmin radius and for the SIS a region of about 5 arcmin radius which extended partially outside the detector boundaries; in the latter case we integrated inside the largest possible circular region, i.e. 4.2 arcmin radius for the SIS0 (see Fig. 1) and 3.4 arcmin radius for the SIS1. Typical SIS and GIS count rates were 2 cts/s and 0.9 cts/s, respectively. The spectral channels were rebinned to get at least 20 cts per bin. The background spectra were accumulated from a source-free region (outside the 98% encircled energy region) large enough to get a good statistics. For the data reduction we used XSELECT V1.3, while the response matrices were update to Nov. 9, 1994 for the SIS and to March 6, 1995

[1] A similar explanation has been suggested for the apparent metal deficiency of active stars derived from Strömgren photometry (e.g. Olsen 1984, Gimémez et al. 1991, Morale et al. 1996)

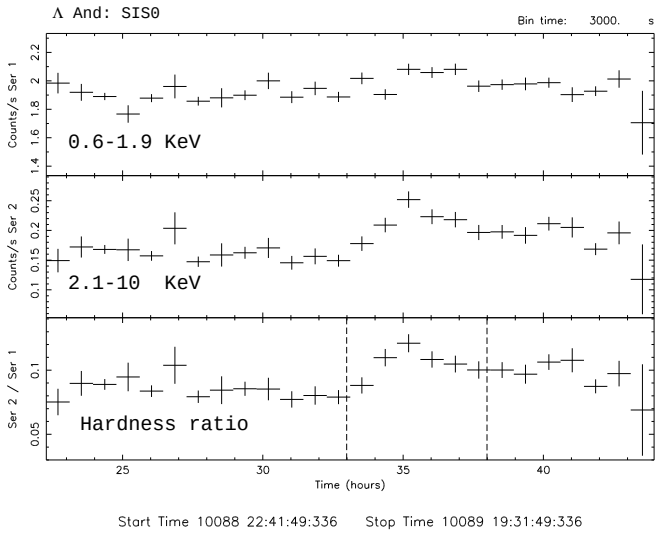

Fig. 2. SIS0 light curves in the energy ranges $0.6-1.9$ keV and $2.1-10$ keV and their hardness ratio. Dashed lines define the time intervals over which we have accumulated different spectra

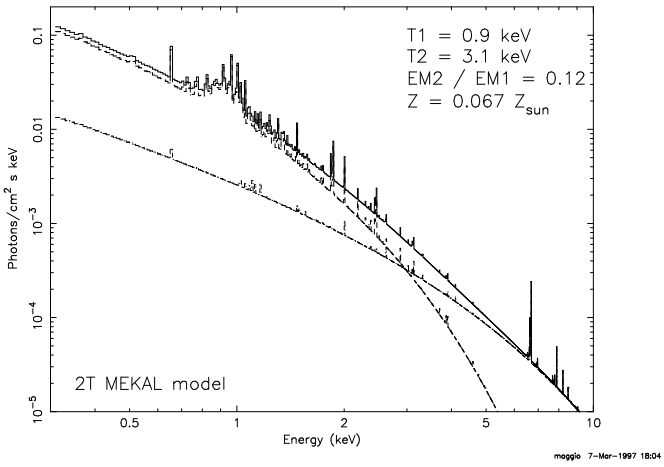

Fig. 3. 2-T MK input model spectrum for the best-fit of the SIS0 total spectrum. The best-fit parameters are indicated

for the GIS. Auxiliary response files (ARF's) were computed with the utility *ascaarf* V2.50 of the package FTOOLS V3.4.

2.2. Light curve analysis

We have analyzed the light curves for the 4 different detectors. For all of them the count rates were not consistent with a constant source and showed variations of about 15% on a time scale of a few hours with no obvious flare. A simple χ^2 test on the total count rate, binned at intervals of 300 sec, yielded a probability of the order of 1×10^{-9} that the source is constant (reduced $\chi^2 = 2.2$ with 100 degrees of freedom). Probabilities of 4×10^{-5} and 1×10^{-6} where obtained for the separate energy ranges 0.6-1.9 keV and 2.1-10 keV which we considered in order to test a possible energy dependence of the source variability. The hardness ratio showed a slight but significant variation for the SIS data (Fig. 2), whereas the variation was close to the 1-σ error for the GIS detectors. Given this small-amplitude but significant variability we divided the total integration time into three subintervals as shown in Fig. 2 and we accumulated spectra for each subinterval in addition to the total spectrum.

2.3. Spectral analysis

For the spectral analysis we used the line + continuum models of Mewe et al. (1995; hereafter MK) and Raymond & Smith (1977; hereafter RS), as implemented in the spectral analysis package XSPEC V9.00. Both models are physically appropriate for optically thin coronal plasmas in collisional equilibrium. Note that the Mewe et al. model used by us is the one indicated in XSPEC as MEKAL. It updates a previous version of the same code (known as MEKA) by using the ionization balance of Arnaud & Raymond (1992) for iron, improved calculations for Fe L-shell transitions, and addition of a number of dielectronic satellite lines. On the other hand, the version of the Raymond & Smith spectrum implemented in XSPEC is the last publicly released version (December 1991) and it does not include some of the latest (unpublished) updates to the code.

For the count errors we adopted the approximation of Gehrels (1986) for data following the Poisson statistics, instead of the less accurate Gaussian approximation.

In the following, we will discuss separately the results for the SIS and GIS detectors, as well as the results of the combined analysis of the two data sets (SIS+GIS). The fits to these data were obtained, in general, with a two-temperature (2-T) model and free metallicity Z relative to the solar value, i.e. we have assumed that the abundances of all elements vary in the same ratio with respect to the corresponding photospheric values. In the only case of the SIS spectra we have also performed the analysis with individual element abundances left free to vary. In all fits, the interstellar absorption parameter $N_{\rm H}$ was fixed at 1×10^{19} cm^{-2}, as measured from the ROSAT data (see Sect. 3.1).

2.3.1. Analysis of the SIS data

We analyzed the SIS data over the spectral range 0.55-10 keV. In fact, spectral channels at higher energies were dominated by noise due to the rapid effective area decrease, while SIS channels with energy less than 0.55 keV have relevant calibration uncertainties (Dotani et al. 1996). No acceptable fit, in fact, was obtained including the low-energy channels both in terms of χ^2 values and of the distribution of residuals. Moreover, the results of the fit appeared strictly dependent on the number of these channels, if included.

As shown in Fig. 3, the 2-T MK model needed to fit the total SIS0 spectrum (but similar results were obtained for the RS model and for all SIS spectra) consists of a low-temperature component, responsible for most of the line emission, plus a high-energy tail, in analogy with other ASCA coronal observations (e.g. Antunes et al. 1994, Gotthelf et al. 1994, White

et al. 1994, Drake et al. 1994, Singh et al. 1995). Reduced χ^2 values greater than 3 were obtained using a 1-T model, while a 3-T model in no case improved the goodness of the fit and the parameters of the third component were always unconstrained. All fits (including the non-acceptable 1-T and 3-T models) depended critically on the Z parameter for which we obtained consistently a sub-solar value $Z \simeq 7 \times 10^{-2}$.

In Table 1 we report the results of the spectral analysis of the entire observation, performed with 2-T MK and RS models. We give results for SIS0 and SIS1 separately as well as for the combined analysis of the two detectors. Errors are computed at the 90% confidence level considering four interesting parameters (T_1, T_2, EM_1/EM_2 and Z), i.e. a confidence region based on $\Delta\chi^2$ =7.78 (Avni, 1976). No significant difference can be seen from the comparison of the MK and RS fits, as well as of the SIS0 and SIS1 fits.

Although these SIS fits can look acceptable in terms of $\chi^2_{\rm red}$ and of the distribution of residuals, an inspection of the last column of Table 1, where the χ^2 probability is given, shows that these fits are unsatisfactory from a statistical point of view, given the large number of degrees of freedom. This problem could arise from calibration errors as well as from inaccuracies in the current plasma models; these uncertainties are expected to be detectable only in the high-resolution SIS spectra. To investigate this issue, we have performed fits to the SIS0 data using a 2-T MK model and adding increasing amounts of systematic errors[2] to all channels (from 1% to 6%). As shown in Table 2, a systematic error of only 4% is sufficient to get acceptable fits to the SIS spectra, since the resulting decrease of the best-fit $\chi^2_{\rm red}$ from 1.3 to 1.1 makes the χ^2 probability acceptable, while leaving the best-fit parameters virtually unchanged. Systematic errors at this level are very likely to be present in the SIS data as well as in the spectral models adopted.

The results of the time-resolved analysis (over the intervals specified in Sect. 3) are reported in Fig. 4 for the SIS0 data. A 2-T MK model has been assumed fixing the metallicity Z to the constant value 0.075. All parameter variations are within their uncertainties, so no significant spectral change emerges from the analysis.

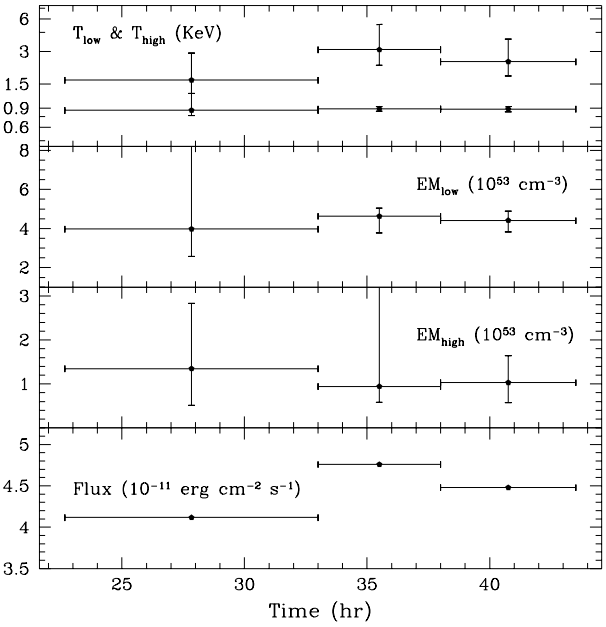

Fig. 4. Time-resolved analysis of SIS0 spectra with a 2-T MK model and metallicity fixed to 0.075 solar. The flux is over the band 0.6 - 10 keV

2.3.2. Analysis of the SIS spectra with free individual abundances

Several authors have fitted ASCA spectra of coronal sources with thermal models in which the elemental abundances are allowed to vary individually, rather than in a constant proportion with respect to the solar values (e.g. White et al. 1994, Drake et al. 1994, Mewe et al. 1996, Tagliaferri et al. 1996). We have attempted the same approach only for the SIS spectra. The results are given in Table 3 for 2-T MK and RS models, for both the SIS0 spectrum and the SIS0+SIS1. We have considered as free parameters only the ions which contribute most to line emission in the ASCA passband. These include O, Ne, Mg, Si, S, Fe and Ni, whose abundances can be sufficiently well constrained. Similar fits made by adding N, Ar and Ca as free parameters resulted in abundances for these elements that were unconstrained. The abundances of all other elements, including a few like Na and Al which contribute (albeit modestly) to the ASCA passband, were frozen to the solar value. Errors were calculated at the 90% confidence level for only one interesting parameter (i.e. $\Delta\chi^2$ = 2.76), thus they result rather small in Table 3. Note that the fits in Table 3 do not include systematic errors.

As shown by a comparison of Tables 1 and 3, there is no significant improvement in the quality of the fits by leaving the individual abundances free to vary. The fits of SIS spectra with a variable Z metallicity were formally unsatisfactory in terms of χ^2 probability (see Table 1), and this is also true for the fits in Table 3. Rather than varying the abundances of individual elements, one can get acceptable fits by adding more realistically a few percent systematic error to the SIS spectra, as we have discussed above. In any case, the fits in Table 3 show

[2] These additional uncertainties are treated, in practice, as random errors added in quadrature to the purely statistical errors. The true, systematic calibration errors are difficult to estimate and to account for because the uncertainties in neighboring energy bins may be correlated in complex ways. The same can be said for the uncertainties in the plasma emissivity models, due mainly to errors in the atomic parameters. Note that XSPEC V9.0 allows adding systematic and statistical errors in quadrature only if the latter are computed in the Gaussian approximation, not according to Gehrels; as a consequence, the total (Gaussian plus systematic) errors may be slightly lower than the Gehrels errors, yielding higher χ^2 values and hence lower probabilities than in the case of no systematic errors, unless these errors are large enough.

Table 1. Best-fit parameters for the SIS spectra computed for 2-T MK and RS models and free metallicity. The hydrogen column density has been fixed to 1×10^{19} cm^{-2}, as suggested by the best fit of the ROSAT PSPC spectrum. Errors are at 90% confidence level for 4 parameters of interest. The flux was evaluated in the 0.6 - 10 keV band.

Detector/ Model	T_1 (keV)	EM_1 (10^{53} cm^{-3})	T_2 (keV)	EM_2 (10^{53} cm^{-3})	Z ($Z_\odot/100$)	Flux (erg cm^{-2} s^{-1})	χ^2_{red}	d.o.f.	Prob. (%)
SIS0									
2MK	$0.90\pm^{0.02}_{0.04}$	$4.85\pm^{0.52}_{0.96}$	$3.1\pm^{2.6}_{1.1}$	$0.67\pm^{0.57}_{0.28}$	$6.7\pm^{1.7}_{0.7}$	$4.4 \cdot 10^{-11}$	1.3	165	0.2
2RS	$0.90\pm^{0.02}_{0.01}$	$4.75\pm^{0.48}_{0.54}$	$3.3\pm^{1.9}_{0.9}$	$0.66\pm^{0.29}_{0.22}$	$8.0\pm^{1.3}_{1.1}$	$4.5 \cdot 10^{-11}$	1.2	165	1.7
SIS1									
2MK	$0.89\pm^{0.05}_{0.04}$	$3.54\pm^{0.50}_{0.82}$	$1.9\pm^{0.9}_{0.3}$	$1.37\pm^{0.59}_{0.71}$	$9.8\pm^{2.2}_{2.0}$	$4.3 \cdot 10^{-11}$	1.6	151	< 0.01
2RS	$0.90\pm^{0.03}_{0.01}$	$3.98\pm^{0.48}_{0.60}$	$2.3\pm^{0.7}_{0.4}$	$0.97\pm^{0.33}_{0.31}$	$10.3\pm^{2.0}_{1.3}$	$4.4 \cdot 10^{-11}$	1.5	151	< 0.01
SIS0 & SIS1									
2MK	$0.90\pm^{0.02}_{0.04}$	$4.30\pm^{0.55}_{1.04}$	$2.4\pm^{1.0}_{0.6}$	$0.93\pm^{0.60}_{0.36}$	$8.0\pm^{2.0}_{1.0}$		1.6	321	< 0.01
2RS	$0.90\pm^{0.01}_{0.01}$	$4.37\pm^{0.37}_{0.41}$	$2.7\pm^{0.7}_{0.4}$	$0.81\pm^{0.22}_{0.21}$	$9.0\pm^{1.0}_{1.0}$		1.5	321	< 0.01

Table 2. Best-fit parameters of the SIS0 spectrum computed for a 2-T MK model and various amounts of systematic errors. Errors are at 90% confidence level for 4 parameters of interest.

Syst. Error	T_1 (keV)	EM_1 (10^{53} cm^{-3})	T_2 (keV)	EM_2 (10^{53} cm^{-3})	Z ($Z_\odot/100$)	χ^2_{red} 165 d.o.f.	Prob. (%)
1%	$0.90\pm^{0.02}_{0.04}$	$4.78\pm^{0.50}_{0.79}$	$3.0\pm^{1.9}_{0.9}$	$0.70\pm^{0.50}_{0.28}$	$7.0\pm^{1.4}_{0.9}$	1.6	< 0.01
2%	$0.89\pm^{0.04}_{0.03}$	$4.68\pm^{0.55}_{0.86}$	$2.9\pm^{1.9}_{0.8}$	$0.74\pm^{0.55}_{0.31}$	$7.2\pm^{1.7}_{1.1}$	1.4	0.08
3%	$0.89\pm^{0.04}_{0.04}$	$4.58\pm^{0.61}_{0.96}$	$2.9\pm^{1.8}_{0.9}$	$0.77\pm^{0.61}_{0.34}$	$7.4\pm^{2.0}_{1.2}$	1.2	3.4
4%	$0.89\pm^{0.05}_{0.05}$	$4.53\pm^{0.66}_{1.05}$	$2.8\pm^{2.0}_{0.8}$	$0.80\pm^{0.67}_{0.37}$	$7.6\pm^{2.4}_{1.5}$	1.1	24.8
5%	$0.89\pm^{0.05}_{0.06}$	$4.47\pm^{0.73}_{1.13}$	$2.8\pm^{2.1}_{0.9}$	$0.81\pm^{0.72}_{0.40}$	$7.8\pm^{2.7}_{1.7}$	1.0	61.3
6%	$0.89\pm^{0.06}_{0.07}$	$4.44\pm^{0.78}_{1.23}$	$2.8\pm^{2.2}_{0.9}$	$0.82\pm^{0.78}_{0.42}$	$7.9\pm^{3.1}_{1.9}$	0.9	86.7

Table 3. Best-fit parameters for the SIS spectra computed for 2-T MK and RS models and individual abundances left free to vary. Only elements which contribute most to line emission in the ASCA passband have been considered, the abundances of the other elements been frozen to the solar value. Similar results are obtained by considering also N, Ar, Ca, but the abundances of these elements result unconstrained. The hydrogen column density has been fixed to 1×10^{19} cm^{-2}, as suggested by a best fit of the ROSAT PSPC spectrum. Errors are at 90% confidence level for one parameter of interest ($\Delta\chi^2$= 2.76).

Parameter		**SIS0** 2MK	**SIS0** 2RS	**SIS0 & SIS1** 2MK	**SIS0 & SIS1** 2RS
T_1	(keV)	$0.76\pm^{0.02}_{0.02}$	$0.88\pm^{0.01}_{0.01}$	$0.78\pm^{0.02}_{0.02}$	$0.89\pm^{0.01}_{0.01}$
EM_1	(10^{53} cm^{-3})	3.78	4.68	3.78	4.57
T_2	(keV)	$2.5\pm^{0.5}_{0.3}$	$3.7\pm^{1.4}_{0.6}$	$2.4\pm^{0.6}_{0.3}$	$3.5\pm^{0.7}_{0.6}$
EM_2	(10^{53} cm^{-3})	0.99	0.53	0.98	0.55
O	(FIP = 13.6 eV)	$0.06\pm^{0.04}_{0.04}$	$0.02\pm^{0.04}_{0.02}$	$0.02\pm^{0.03}_{0.02}$	$0.00\pm^{0.01}_{0.00}$
Ne	(FIP = 21.6 eV)	$0.35\pm^{0.05}_{0.05}$	$0.07\pm^{0.06}_{0.07}$	$0.35\pm^{0.04}_{0.04}$	$0.08\pm^{0.05}_{0.05}$
Mg	(FIP = 7.6 eV)	$0.23\pm^{0.04}_{0.04}$	$0.12\pm^{0.03}_{0.03}$	$0.24\pm^{0.03}_{0.03}$	$0.15\pm^{0.02}_{0.02}$
Si	(FIP = 8.2 eV)	$0.16\pm^{0.03}_{0.03}$	$0.10\pm^{0.02}_{0.02}$	$0.17\pm^{0.02}_{0.02}$	$0.11\pm^{0.02}_{0.02}$
S	(FIP = 10.4 eV)	$0.18\pm^{0.08}_{0.07}$	$0.11\pm^{0.05}_{0.05}$	$0.16\pm^{0.05}_{0.05}$	$0.11\pm^{0.04}_{0.04}$
Fe	(FIP = 7.9 eV)	$0.07\pm^{0.01}_{0.01}$	$0.07\pm^{0.01}_{0.01}$	$0.07\pm^{0.01}_{0.01}$	$0.08\pm^{0.01}_{0.01}$
Ni	(FIP = 7.6 eV)	$0.47\pm^{0.16}_{0.15}$	$0.24\pm^{0.08}_{0.08}$	$0.43\pm^{0.11}_{0.11}$	$0.26\pm^{0.06}_{0.06}$
χ^2_{red}		1.37	1.39	1.46	1.44
d.o.f.		159		315	

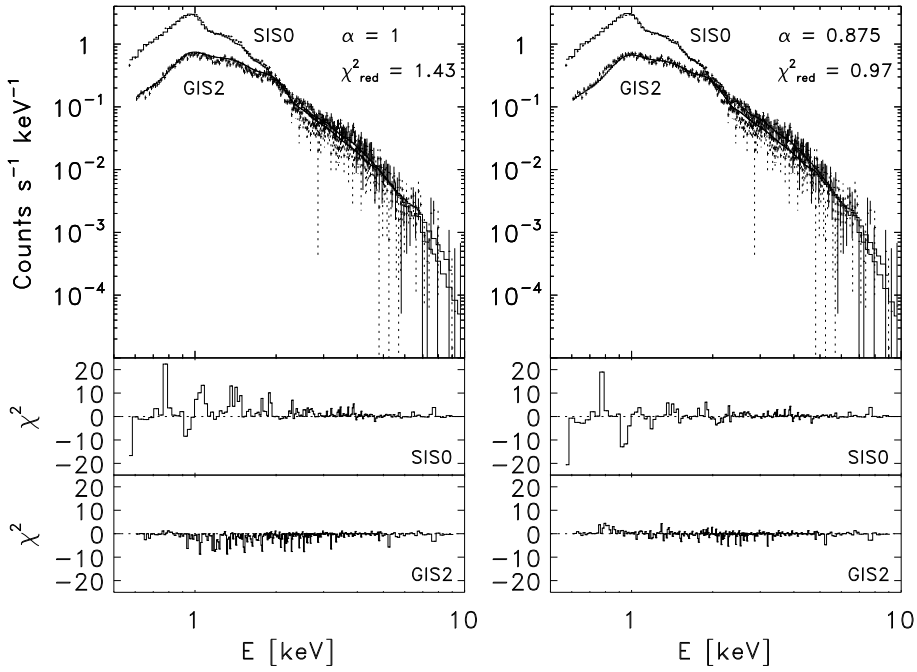

Fig. 5. Best-fit of the spectra of the two best calibrated detectors, SIS0 & GIS2, fitted simultaneously with a 2-T MK model and free metallicity. On the left, no normalization factor has been introduced for the relative response of the two detectors. On the right, a normalization factor α = 0.875 has been introduced. Note the difference in the distribution of residuals and in the χ^2_{red} values

that *all* elements are underabundant with respect to solar (typically by factors between $\sim$ 0.1 to 0.3). Note that by leaving the abundances of individual elements free to vary, uncertainties in the adopted plasma model become critical (see the differences found for some elements by using the MK or the RS models, especially Ne and Mg, probably reflecting the differences between the two codes in the calculation of the Fe-L shell line complex at $\sim$ 1 keV), and the results may also depend significantly on the elements left free to vary (as we have verified for example by either fixing the Ni abundance to the solar value or allowing it to vary). Since the continuum is not well determined in these data (for lack of photons at energies higher than $\sim$ 2 keV), it is difficult to disentangle the contributions of emission measure and elemental abundances to the measured fluxes in the various lines. More importantly, there is no need to vary the abundances of individual elements (rather than the overall metallicity), if a modest amount of systematic uncertainties is included.

2.3.3. Analysis of the GIS data

Considering the effective area of the GIS detectors, we have chosen to analyze the GIS data over the spectral range $0.6 - 10$ keV to be consistent with the selected SIS spectral range.

If we take into account only the $\chi^2_{\rm red}$ value, which is of the order of unity, the GIS spectra could be reproduced by a 1-T model (with both the MK and RS models), which corresponds to the low-temperature component of the SIS spectral fits. However, at energies higher than $\sim$ 3 keV the systematically positive residuals suggest the need of a high-temperature component in the model, consistently with the higher resolution SIS data. The addition of such a component not only reduces the χ^2 value, but also makes the distribution of residuals more stochastic. The results of 2-T fits of the GIS data are given in Table 4. Owing to the worse energy resolution and sensitivity of the GIS relative to the SIS, we obtained less constrained parameters which are consistent, within their larger uncertainties, with those found from the SIS data. The χ^2 probability is now completely acceptable, even ignoring systematic errors (which however are likely to be present). The same can be said of the time-resolved analysis which gave results similar to the time-resolved SIS analysis, albeit with larger errors.

2.3.4. Combined analysis of SIS0 and GIS2 data

We then attempted to fit simultaneously the total spectra of SIS0 and GIS2, which are considered to be the best calibrated ASCA detectors. In so doing, we first obtained a non satisfactory fit (with no systematic errors added): the derived $\chi^2_{\rm red}$ of $\sim$ 1.3 has in fact an extremely low probability due to the large number of degrees of freedom. The fits of the time-resolved spectra were more acceptable, but simply because the larger relative errors (due to the lower number of counts) reduced the final χ^2 value. All fits (for both the total observation and the time-resolved spectra) showed a distribution of residuals systematically above and below the zero line for the SIS0 and GIS2, respectively (see Fig. 5, left-hand panel). At the same time, we found that the fluxes measured from the GIS2 spectra resulted systematically underestimated by a factor 0.8-0.9 with respect to the ones measured from the SIS0 spectra.

From this we inferred the presence of a flux calibration difference between the SIS0 and GIS2 responsible for the resulting distribution of residuals. To cope with this problem, we introduced a multiplicative factor α for the relative normalization of the two spectra, in such a way as to minimize the χ^2 values. We were able to get significantly lower χ^2 values adopting α = 0.875, in agreement with the measured flux ratio for the two

Table 4. Best-fit parameters for the GIS spectra computed for 2-T MK and RS models and free metallicity. Errors are at 90% confidence level for 4 parameters of interest. The flux was evaluated in the 0.6 - 10 keV band.

Detector/ Model	T_1 (keV)	EM_1 (10^{53} cm^{-3})	T_2 (keV)	EM_2 (10^{53} cm^{-3})	Z ($Z_\odot/100$)	Flux (erg cm^{-2} s^{-1})	χ^2_{red}	d.o.f.	Prob. (%)
GIS2									
2MK	$0.81\pm^{0.08}_{0.09}$	$4.65\pm^{1.07}_{1.51}$	$2.8\pm^{3.1}_{1.1}$	$0.64\pm^{0.83}_{0.36}$	$6.6\pm^{3.9}_{2.2}$	$4.0 \cdot 10^{-11}$	0.7	298	> 99
2RS	$0.85\pm^{0.04}_{0.06}$	$4.53\pm^{0.97}_{1.26}$	$3.2\pm^{4.1}_{1.3}$	$0.50\pm^{0.56}_{0.26}$	$7.5\pm^{4.1}_{2.6}$	$4.0 \cdot 10^{-11}$	0.7	298	> 99
GIS3									
2MK	$0.95\pm^{0.07}_{0.09}$	$4.02\pm^{0.82}_{1.43}$	$2.6\pm^{5.1}_{1.0}$	$0.55\pm^{0.99}_{0.38}$	$8.6\pm^{4.2}_{2.6}$	$3.9 \cdot 10^{-11}$	0.7	309	> 99
2RS	$0.92\pm^{0.08}_{0.04}$	$3.94\pm^{0.94}_{1.33}$	$2.5\pm^{4.9}_{0.8}$	$0.64\pm^{0.72}_{0.47}$	$9.7\pm^{5.4}_{3.2}$	$3.9 \cdot 10^{-11}$	0.8	309	> 99
GIS2 & GIS3									
2MK	$0.89\pm^{0.06}_{0.06}$	$4.26\pm^{0.65}_{0.90}$	$2.8\pm^{2.0}_{0.9}$	$0.57\pm^{0.55}_{0.28}$	$7.7\pm^{2.5}_{1.8}$		0.7	612	> 99
2RS	$0.89\pm^{0.05}_{0.03}$	$4.26\pm^{0.61}_{0.85}$	$2.9\pm^{1.9}_{0.9}$	$0.52\pm^{0.41}_{0.23}$	$8.6\pm^{2.8}_{2.0}$		0.8	612	> 99

Table 5. Best-fit parameters for the combined analysis of SIS0 & GIS2 spectra, with and without a 4% systematic error. The fits are computed for 2-T MK and RS models and free metallicity, assuming a relative normalization factor $\alpha = EM_{\rm GIS2} \ / \ EM_{\rm SIS0} = 0.875$ between the two detectors. The emission measures refer to the SIS0 spectrum and are 1.14 times the GIS2 ones. Errors are at 90% confidence level for 4 parameters of interest.

SIS0 & GIS2 Model	T_1 (KeV)	EM_1 ($10^{53} cm^{-3}$)	T_2 (KeV)	EM_2 ($10^{53} cm^{-3}$)	Z ($Z_\odot/100$)	χ^2_{red} 468 d.o.f.	Prob. (%)
2MK	$0.90\pm^{0.02}_{0.02}$	$4.98\pm^{0.42}_{0.64}$	$3.3\pm^{1.9}_{1.0}$	$0.59\pm^{0.40}_{0.22}$	$6.8\pm^{1.1}_{0.8}$	1.0	63
2RS	$0.90\pm^{0.01}_{0.01}$	$4.86\pm^{0.41}_{0.48}$	$3.4\pm^{1.7}_{0.9}$	$0.58\pm^{0.24}_{0.17}$	$7.9\pm^{1.2}_{0.9}$	0.9	77
SYS. ERR. = 4%							
2MK	$0.88\pm^{0.04}_{0.03}$	$4.73\pm^{0.49}_{0.67}$	$3.0\pm^{1.4}_{0.8}$	$0.67\pm^{0.43}_{0.25}$	$7.7\pm^{2.3}_{1.2}$	1.0	37
2RS	$0.89\pm^{0.03}_{0.01}$	$4.70\pm^{0.47}_{0.55}$	$3.3\pm^{1.3}_{0.8}$	$0.60\pm^{0.25}_{0.18}$	$8.7\pm^{1.6}_{1.4}$	1.0	41

detectors.[3] This also gave the stochastic distribution of residuals expected from an acceptable fit (cf. Fig. 5, right-hand panel).

Fitting together the SIS0 and GIS2 data we obtained values that were similar, but better constrained, than the ones obtained with the SIS or GIS separately (cf. Table 5, upper part). Also the χ^2 probability is much better than for the SIS data alone, indicating an acceptable fit, even without including systematic errors (except for the normalization factor discussed above). We emphasize that the confidence limits in Table 5 are at 90% for 4 interesting parameters, so they represent the maximum range of parameter indetermination at that confidence level. However, systematic errors, not taken into account, are likely to be present and will increase the uncertainty on the computed values.

As an estimate of residual calibration uncertainties, as well as of possible uncertainties in the adopted spectral code, we have assumed a 4% systematic error for each spectral channel, as indicated by the analysis of the SIS data (see Sect. 2.3.1). The results obtained by adding this systematic error to the SIS0 and GIS2 data are given in the lower part of Table 5. The apparently surprising better definition of the high-temperature component when systematic errors are added (see Table 5) depends on the fact that the Gaussian plus systematic errors are lower in the high-energy channels than the errors computed with the Gehrels approximation. For the same reason, the χ^2 probability is slightly larger in the latter case.

In Figs. 6 and 7 we plot the confidence contours for various parameters. In particular, we show contour plots of Z versus T_2 for different T_1 values for the simultaneous fits of SIS0 & GIS2 data, with and without systematic errors.

3. The ROSAT data

λ And was observed also by the PSPC detector on board ROSAT, once during the *All Sky Survey*, and a second time during a long pointed observation that we have retrieved from the public archive.

[3] The cross-calibration discrepancy between the SIS and GIS detectors can now be corrected using ARF's generated with the most recent release of the utility *ascaarf* (later than V2.62).

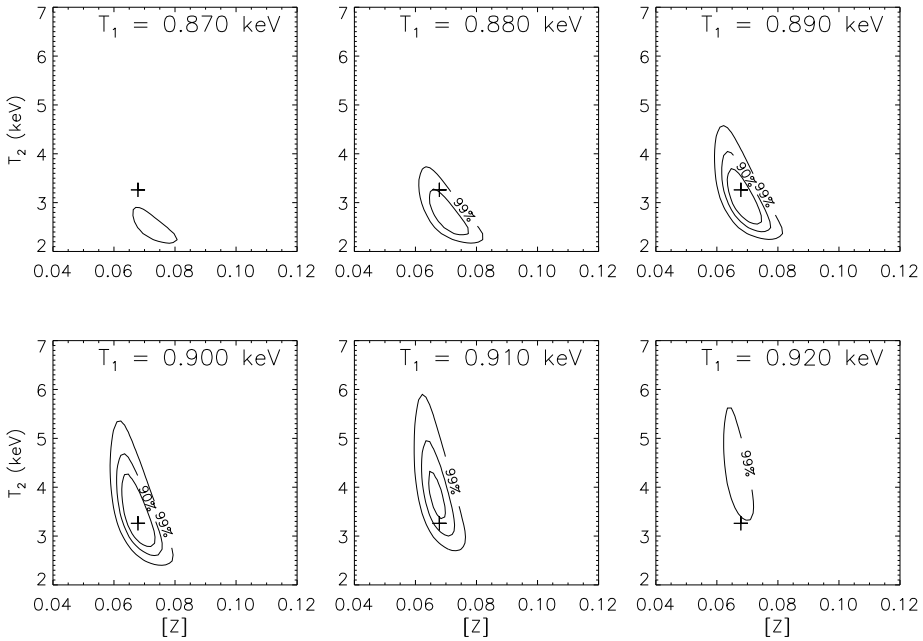

Fig. 6. Contour plots of T_2 versus Z for different T_1 values for the simultaneous best-fit of the SIS0 & GIS2 spectra, without systematic errors added

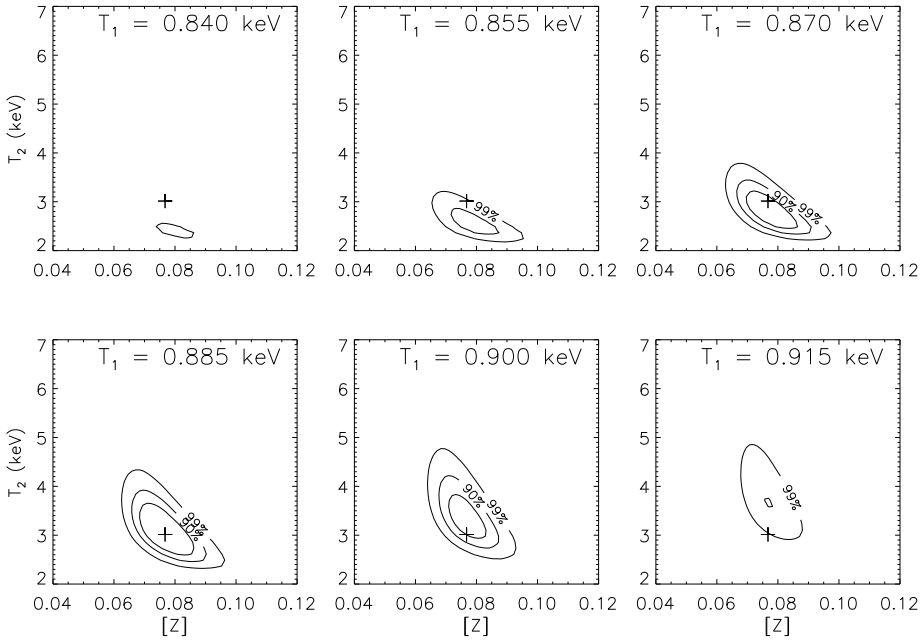

Fig. 7. Similar to Fig. 6, but with a 4% systematic error included. Note the different range of T_1 considered, with respect to Fig. 6

The *All Sky Survey* observation was analyzed by Dempsey et al. (1993a,b) who derived the following values for the best-fit parameters and related confidence ranges (at the 90% level for one interesting parameter): T_1 = 0.084 keV, ΔT_1 = 0.083 − 0.27 keV, T_2 = 1.67 keV, ΔT_2 = 1.36 − 2.16 keV, EM_1/EM_2 = 0.1 (with no error given), $N_{\rm H}$ = 1.1 × 10^{19} cm^{-2}, $\chi^2_{\rm red}$ = 0.99. Note that these values (particularly the small low-temperature component) are significantly different from those obtained by us from the ASCA spectra as well as from the pointed ROSAT observation (see later). In addition, the metallicity Z was fixed to the solar value.

3.1. ROSAT pointed observation

The ROSAT pointed observation of λ And was obtained on July 9-10, 1991, $\sim$ 4.5 years earlier than the ASCA observation. It had a total useful integration time of 32 ksec, during which a total of $\sim$ 250,000 cts were collected in the energy range 0.1 - 2.4 keV. In order to fix an error in the spatial gain correction, introduced by the standard ROSAT data processing (SASS), we have reprocessed the PSPC event file with the tool PCPICOR (in the package FTOOLS V3.4), as recommended by Snowden et al. (1995). The source spectrum was then extracted from a circle of 3 arcmin radius around the X-ray centroid. The background was accumulated in a concentric annulus extending from 4 to 8

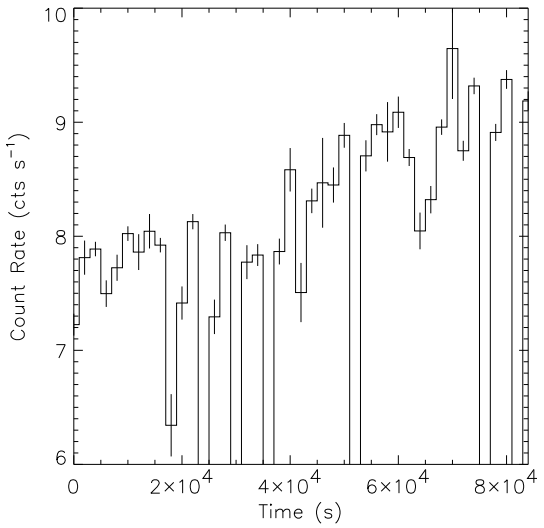

Fig. 8. Light curve of the *ROSAT* PSPC pointed observation

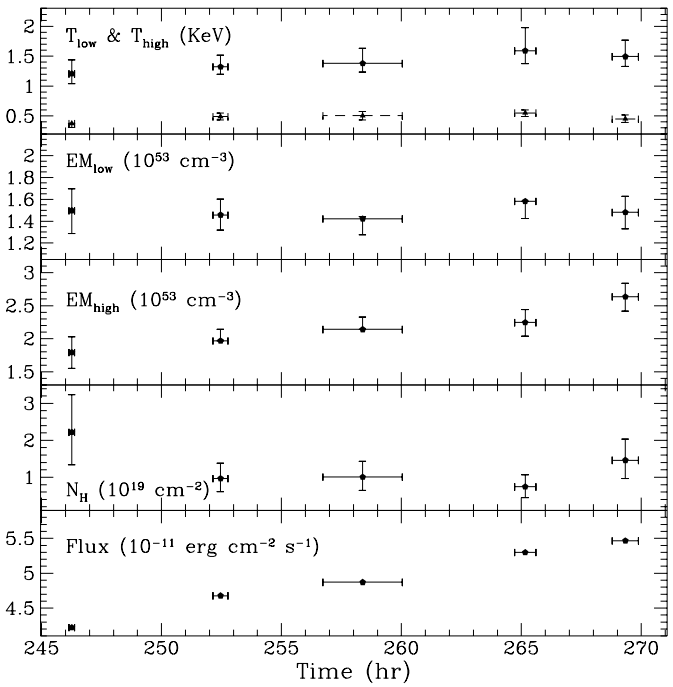

Fig. 9. Time-resolved analysis of the PSPC spectra with a 2-T MK model and metallicity fixed to 0.25 solar. The flux is computed in the band 0.3-3 keV

arcmin. The ROSAT light curve is shown in Fig. 8. It shows an increase by $\sim$ 30% of the count rate throughout the observation and an overall variability significant at the 99% confidence level, according to both Kolmogorov-Smirnov and Cramer-von-Mises statistical tests as implemented within PROS V2.10.4. However, no obvious flare-like event is evident.

For the spectral analysis, we have adopted the so called "92MAR11" PSPC response matrix, recommended for observations taken before the gain change of the PSPC that occurred on Oct 1991. The first two energy bins, in the standard 34-bin scheme, were ignored because they are poorly calibrated. We have tested that the results reported below are only slightly affected if one or two more bins are ignored, in addition to the first two, likely because the smaller energy band reduces the ability of the spectral fitting to constrain the interstellar absorption and the plasma metallicity. The total integrated spectrum for the whole observation was fitted with 1-T and 2-T MK and RS models, with variable column density, $N_{\rm H}$, and variable metallicity, Z. No attempt was made to change the abundances of individual elements, since this was not warranted by the PSPC low-resolution (see discussion on this point in Sect. 2.3.2 in relation to the ASCA SIS data).

No good fit was obtained with any of the models ($\chi^2_{\rm red} \simeq 5$), taking into account the poissonian errors only, and no significant improvement could be obtained by adding further thermal components. In low-resolution spectra such as those provided by the PSPC, high $\chi^2_{\rm red}$ values are unlikely to be due to uncertainties in the model; rather, we interpret this result as a consequence of the high statistics of our spectrum which leads to poissonian errors comparable to or less than other sources of uncertainty. In particular, a calibration error of $\sim$ 2% is expected to affect on average each spectral channel and should be taken into account (Fiore et al. 1994, Bocchino et al. 1994).

Even assuming such an additional error no acceptable fit was possible with 1-T models, or by fixing Z to the solar value. We were able to obtain acceptable fits (see Table 6) with 2-T RS and MK models with variable Z; the best-fit parameters were in agreement for the two models within the confidence ranges. These ranges were computed at the 90% confidence level for 5 interesting parameters (T_1, T_2, EM_1/EM_2, Z, $N_{\rm H}$) which means a $\Delta\chi^2$ = 9.2. The temperatures of both components were well constrained, as well as the hydrogen column density (for which the photo-electric cross-sections of Morrison & McCammon 1983 were adopted), and the overall metallicity.

The derived metallicity ($\approx$ 0.25 solar) is significantly larger (by a factor $\sim$ 3) than indicated by the ASCA data. The $N_{\rm H}$ value is much better constrained by ROSAT than by ASCA, and this is the reason why we used the ROSAT $N_{\rm H}$ value also in fitting the ASCA spectra.

As the PSPC light curve showed significant variability, we searched for variations of the coronal parameters by sampling uniformly the observation over a few short time intervals (each of $\sim 1-2$ ksec duration). We fixed the metallicity Z to the value found for the total observation. The time-resolved spectra could be fitted with 2-T models with temperatures similar to those found from the analysis of the total observation, but with a monotonic increase of EM_2 by $\sim$ 47%, which largely explains the $\sim$ 30% monotonic increase of the X-ray flux in the ROSAT band. No significant variation could be found for the other parameters (see Fig. 9).

In summary, three points need to be emphasised:

1) The metallicity derived from the ROSAT fit is about 2-3 times larger than indicated by the ASCA data. We were unable to find an acceptable fit to the PSPC spectrum by forcing Z

Table 6. Best-fit parameters for the PSPC spectrum computed for 2-T MK and RS models, with metallicity and hydrogen column density free to vary. A 2% systematic error has been added to the PSPC spectrum. Errors are at 90% confidence level for 5 parameters of interest: nc means non-constrained parameter. The flux was evaluated in the 0.6 - 10 keV band, for comparison with the ASCA results.

PSPC	SYST. ERRORS = 2%								
Model	T_1 (keV)	EM_1 (10^{53} cm^{-3})	T_2 (keV)	EM_2 (10^{53} cm^{-3})	Z ($Z_\odot/100$)	$N_{\rm H}$ (10^{19} cm^{-2})	Flux (erg cm^{-2} s^{-1})	χ^2_{red} 26 d.o.f.	Prob. (%)
2MK	$0.49\pm^{0.09}_{0.09}$	$1.47\pm^{nc}_{0.31}$	$1.4\pm^{0.2}_{0.1}$	$2.20\pm^{0.20}_{0.22}$	$25.4\pm^{9.5}_{5.4}$	$1.01\pm^{0.69}_{0.69}$	$4.3 \cdot 10^{-11}$	1.4	7
2RS	$0.44\pm^{0.11}_{0.08}$	$1.11\pm^{0.29}_{0.14}$	$1.2\pm^{0.1}_{0.1}$	$2.70\pm^{nc}_{0.21}$	$23.8\pm^{8.0}_{5.9}$	$1.45\pm^{0.59}_{0.61}$	$4.1 \cdot 10^{-11}$	1.1	32

to 0.1 or less, even with the addition of a third component to the model. A similar metallicity is derived consistently also by fitting separately the soft (0.11 - 0.5 keV) and hard (0.5 - 2.4 keV) parts of the PSPC spectrum.

2) The column density $N_{\rm H}$ is about a factor 2 higher than the value inferred by assuming a constant interstellar hydrogen density of 0.07 cm^{-3} (Paresce 1984) and a distance of 23 pc to λ And. Since $N_{\rm H}$ is poorly determined by ASCA, we have used the ROSAT value also for the ASCA fits.

3) The best-fit temperatures and emission measures derived from ROSAT are different from those derived from ASCA, indicating the presence of plasma cooler ($\simeq 6 \times 10^6$ K) than the one responsible for the emission in the harder ASCA passband. Note also that the dominant hot component in the PSPC spectrum has a temperature and an emission measure intermediate between those derived from ASCA. In spite of this, the X-ray flux computed over the band 0.6 - 10 keV ($\simeq 4.3 \times 10^{-11}$ erg cm^{-2} s^{-1}, corresponding to a luminosity of 2.7×10^{30} erg s^{-1} for a source distance of 23 pc) is consistent with the one measured by ASCA notwithstanding the temporal separation (nearly 5 years) between the two observations. This makes the simultaneous fit of PSPC, SIS0 and GIS2 data of some interest.

3.2. Combined analysis of ROSAT and ASCA data

In Table 7 we give the results of the simultaneous fit of the ROSAT PSPC and the ASCA SIS0 and GIS2 data obtained with 2-T MK and RS models. A 2% and 4% systematic error was added to the ROSAT and ASCA spectra, respectively.

By fitting together the three detectors we were unable to find an acceptable χ^2 probability. The large systematic fluctuations in the distribution of residuals (see Fig. 10), especially for the PSPC data, arise probably from the different metallicities and temperatures required by the ASCA and ROSAT spectra. The joint fit indicates a value $Z \simeq 0.11-0.14$, intermediate between those obtained for the three instruments separately (but closer to the ASCA values). No improvement was achieved by fixing the hydrogen column density to 1×10^{19} cm^{-2} or less (note that the best-fit $N_{\rm H}$, for the joint fit is around $2-3 \times 10^{19}$ cm^{-2}). We have also attempted fits to the joint spectrum with 3-T models, with or without $N_{\rm H}$ as a free parameter: in no case we obtained acceptable fits ($\chi^2_{\rm red} > 1.8$), including freezing Z to either the value indicated by ASCA or that indicated by ROSAT.

The disagreement we have found between ROSAT and ASCA is not totally surprising if we take into account the time lag between the two observations and possible cross-calibration errors between the different detectors. We stress that the systematic errors we have included may partially correct for *relative* calibration uncertainties, but not for *absolute* errors in the instrument responses. On the other hand, since the ASCA and ROSAT observations are not simultaneous, the data do not allow any conclusive investigation of this point. The poor quality of the fit of the combined ROSAT and ASCA observations, in fact, could be either due to real spectral changes occurred between the two observations, or to a variety of other causes, including cross-calibration errors, uncertainties in the spectral code adopted, inadequacy of the simple 2-T and 3-T models assumed, or abundance variations of individual elements that are poorly accounted for by a single scaled metallicity Z. We only note that the discrepancy cannot be removed by simply introducing an energy-independent normalization factor between the ASCA and ROSAT spectra.

4. Discussion and conclusions

From the analysis of spectra measured with the ASCA detectors, and from a different observation by the ROSAT PSPC, we have found that:

- the corona of λ And seen by ASCA is well described by a 2-T model with a main component at $T_1 \simeq 0.9$ keV, well constrained and responsible for the line emission, and a much smaller ($EM_2/EM_1 \sim 0.15$) and less constrained component at $T_2 \simeq 3$ keV;
- the corona seen by ROSAT is again well described by a 2-T model but with significantly different parameters: a cool component at $T_1 \simeq 0.5$ keV and a comparable component ($EM_2/EM_1 \sim 2$) at $T_2 \simeq 1.3$ keV;
- the quiescent, average X-ray flux of the star did not show any substantial change from the ROSAT to the ASCA observation nearly 5 years later, but significant short-term variability was detected during both observations, with a change in flux up to $\sim 30\%$;
- both ASCA and ROSAT indicate a low non-solar metallicity which is consistent with the measured photospheric abundance ($Z_{phot} \sim 0.2$) but differs by about a factor 2

Table 7. Best-fit parameters for the combined analysis of SIS0, GIS2 and PSPC spectra, assuming systematic errors of 4% for the first two detectors and of 2% for the PSPC. The fits refer to 2-T MK and RS models, with metallicity and hydrogen column density free to vary. Systematic errors have been added as indicated at the top of the table. Errors have not been computed because the fit is statistically unacceptable.

	SIS0 GIS2 PSPC							
SYST. ERR. =	4%	4%	2%					
Model	T_1 (keV)	EM_1 (10^{53} cm^{-3})	T_2 (keV)	EM_2 (10^{53} cm^{-3})	Z ($Z_\odot/100$)	$N_{\rm H}$ (10^{19} cm^{-2})	χ^2_{red} 499 d.o.f.	Prob. (%)
2MK	0.7	2.6	1.8	1.8	14.3	2.2	1.8	$< 10^{-6}$
2RS	0.9	3.8	2.6	0.9	11.4	2.7	1.8	$< 10^{-6}$

in the ASCA and ROSAT spectra ($Z \sim 0.1$ and 0.2 solar, respectively);

– the $N_{\rm H}$ value measured by the PSPC detector is about a factor 2 higher than estimated from UV observations (see later). No constraints on $N_{\rm H}$ can be derived from the ASCA spectrum alone.

As shown by the results of our fits, a 2-T model with a scaled non-solar metallicity Z (i.e. with the abundances of all elements reduced in the same proportion with respect to the solar ones) is adequate to reproduce the ASCA and ROSAT spectra, separately. We found that fits of the SIS data alone (with no systematic errors added) were not satisfactory from the point of view of the χ^2 probability, but the addition of a modest amount of systematic uncertainty ($\sim 4\%$) gives completely acceptable results. The fits to the lower-resolution GIS data are satisfactory even without including systematic errors (which however are likely to be present), but give less constrained parameters. The fits to the combined SIS0 & GIS2 data (with and without systematic errors included) are both completely satisfactory, provided we rescale the relative fluxes of the two detectors in order to minimize cross-calibration errors. Finally, the ROSAT PSPC spectra can be fitted satisfactorily by adding the 2% systematic uncertainty derived from other studies (Fiore et al. 1994, Bocchino et al. 1994).

We want to emphasize that more complex models (such as a 3-T model or a power-law continuous emission measure model like CEMEKL implemented in XSPEC) did not allow us to improve the overall quality of the fit. 3-T fits to both ASCA and ROSAT spectra gave a third component poorly constrained and with no influence on the overall model: in fact, the EM of this component was always vanishing small or the temperature very low. The CEMEKL model presented serious convergence problems; even when forced to converge by avoiding the many secondary minima, the χ^2 value was much worse than for a 2-T model with variable Z, and the distribution of residuals was not acceptable. The significantly different coronal parameters that we derived from the ASCA and ROSAT spectra separately could indicate that a continuous emission measure distribution is a more realistic description of the corona of λ And than a simple 2-T model. In fact, a 3-T model to the combined ASCA and ROSAT data, although formally not acceptable ($\chi^2_{\rm red} > 1.8$), suggests the presence of plasma at all temperatures over the range $\simeq 5 \times 10^6 - 3 \times 10^7$ K. However, the different results obtained by fitting the ROSAT and ASCA spectra separately could also indicate that a real spectral change occurred between the two observations (due, e.g., to a different distribution of active regions over the stellar surface), with no significant effect on the total integrated X-ray flux[4]. If this is the case, there is no much point in trying to fit simultaneously the ROSAT and ASCA data.

The finding that the corona of λ And is metal deficient is in line with previous analyses of other ASCA observations of RS CVn binaries (e.g. Gotthelf et al. 1994; White et al. 1994; Drake et al. 1994; Singh et al. 1995, 1996; Mewe et al. 1996; Tagliaferri et al. 1996). Metal underabundance is also required by the ROSAT PSPC data, although the metallicity derived by ROSAT is about a factor of 3 higher than the one derived by ASCA (a similar systematic effect was also found, but not explicitly noticed, by Tagliaferri et al. 1996 in their analysis of the young star HD35850). λ And has been found to have a photospheric metallicity $\simeq 0.16 - 0.25$ solar (Helfer & Wallerstein 1968, Taylor 1991, Tautvaisiene et al. 1992, Randich et al. 1994), in good agreement with the ROSAT metallicity but a factor ~ 2 larger than the ASCA value. Whether this difference between the two fitted coronal values, and between the photospheric and the ASCA metallicity, is significant or not cannot be determined conclusively, because of the possible role played by systematic errors in either the data or the spectral model used. For instance, the same ROSAT observation of λ And discussed here was included in a sample of PSPC coronal sources studied by Bauer & Bregman (1996). These authors derived for λ And a metallicity $Z \sim 0.06$ from a 2-T fit, and coronal parameters significantly different from ours (including an unrealistic value 3.6×10^{20} cm^{-2} for the column density!). Since most of the coronal sources analyzed by them had significantly lower coronal metallicities than the photospheric ones, they questioned the reliability of metallicity determinations with the ROSAT PSPC. Note, however, that the analysis of Bauer & Bregman was based only on the use of the Raymond & Smith spectral code as imple-

[4] The good agreement found by Tagliaferri et al. (1996) between the coronal parameters derived from the ASCA and ROSAT observations of the young star HD35850 suggests that these spectral changes with no significant effect on the total flux may have actually been occurred in the case of λ And

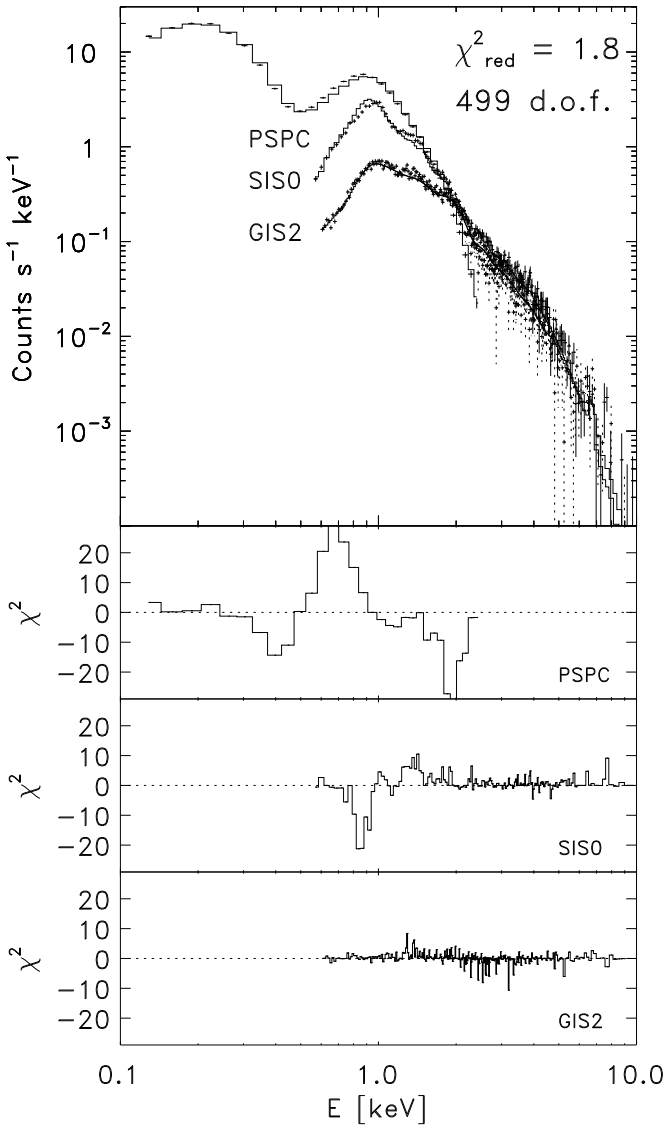

Fig. 10. Simultaneous fit of SIS0, GIS2 and PSPC spectra, with a 2-T MK model and both metallicity and hydrogen column density free to vary. The three lower panels show the distribution of residuals for the PSPC, SIS0 and GIS2, separately. The fit is formally unacceptable (probability $< 10^{-6}$ %

mented in XSPEC V8.50, i.e. with a very incomplete treatment of the Fe lines.

In the solar corona, elements with first ionization potential (FIP) $<$ 10 eV (Fe, Mg, Si, etc.) are observed to be *enhanced* relative to elements with FIP $>$ 10 eV (C, N, O, Ne etc) by average factors of $\sim$ 4 (see, e.g., reviews by Feldman 1992 and Meyer 1993, and references therein). One major question concerns the normalization of the abundance anomaly relative to hydrogen. Feldman (1992; see also Meyer 1993) has argued that the low-FIP species are enhanced relative to H rather than the alternative case in which the high-FIP species are depleted relative to H (both scenarios are observationally equivalent in the absence of indicators of the H abundance). This coronal abundance anomaly is now commonly known as the "FIP effect". Recent studies of stellar coronal abundances with EUVE (Drake et al. 1995, 1996a,b; Schrijver et al. 1995) have revealed solar-like FIP effects in some but not all the stars studied, while ASCA has provided a rather contradictory picture (White et al. 1994, Gotthelf et al. 1994, Drake et al. 1994, Singh et al. 1995, Mewe et al. 1996, Tagliaferri et al. 1996; Güedel et al. 1997). In any case, even if other stars may share the solar coronal abundance anomaly or FIP effect, metal *depletion* as indicated by the RS CVn's and other active stellar coronae is totally opposite to the solar case. For λ And, we confirm the lower metallicity found for other RS CVn binaries, but we are unable to address the question of the FIP effect, since fits with variable abundances are not better than fits obtained by varying all elements in the same proportion (see Sect. 2.3).

Finally, we need to discuss the $N_{\rm H}$ value measured with the ROSAT PSPC which we adopted in all our fits. $N_{\rm H}$ = 1 $\times$ 10^{19} cm^{-2} is about a factor 2 higher than expected for a homogeneous interstellar medium with density $n_H \simeq 0.07$ cm^{-3} (Paresce 1984). Even if the interstellar medium is known not to be uniform, the fitted $N_{\rm H}$ value appears quite high for a star like λ And at only 23 pc. Baliunas & Dupree (1979) derived in fact a value of $4 \pm 2 \times 10^{18}$ cm^{-2} from *Copernicus* observations. The $N_{\rm H}$ value derived from the ROSAT fit is also not consistent with the clear detection of He II (304 Å) line emission in the EUVE/MW spectrum of λ And (Dupree et al. 1996): this result places a fairly strict upper limit on the intervening *neutral* hydrogen column density, $N_{\rm H} < 8 \times 10^{18}$ cm^{-2}, since the ISM transmission at $\simeq$ 300 Å drops abruptly below 10^{-2} for larger $N_{\rm H}$ values. A recent observation of λ And with the GHRS on board the Hubble Space Telescope (Wood et al. 1996) gives for $N_{\rm H}$ a value near the one expected for the average interstellar density ($\sim 4 \times 10^{18}$ cm^{-2}). On the contrary, there is no way we can fit the PSPC spectrum with such a low value and the derived $N_{\rm H}$ appears well constrained (see Table 6). The ASCA spectra provided for $N_{\rm H}$, if this parameter was left free, a value even higher than the PSPC, but absolutely unconstrained.

We can justify such a high "effective" value of $N_{\rm H}$ if we admit the presence of substantial ionization in the ISM, as suggested by many recent studies (see Lallement et al. 1996 for a review). In fact, in the ROSAT soft band (0.11 - 0.28 keV, corresponding to energy bins 3 - 7), the opacity for a cosmic ISM composition is dominated by He rather than by H. While ionized H offers no opacity, ionized He is not too different from He I: any significant ISM ionization gives a higher opacity per neutral H atom, in soft X-rays, than a totally neutral ISM as the one assumed for the photo-electric cross-sections of Morrison & McCammon (1983). The state of the local ISM is not yet well known, but the available evidence could allow for as much as 60% ionization of He (Wood & Linsky 1996). Using the ISM opacity code of Rumph et al. (1994), we have checked that such an ionization fraction could bring the ISM absorption coefficient, due to H I, He I and He II, from a true $N_{\rm H}$ = 4 $\times$ 10^{18} cm^{-2}, to a value close to $N_{\rm H} \simeq 1 \times 10^{19}$ cm^{-2} for a neutral ISM .

λ And has been observed recently by the EUVE satellite. The EUVE results will be presented elsewhere (Drake et al., in preparation). As demonstrated by similar studies on other stellar sources (e.g. Mewe et al. 1996; Güdel et al. 1997), by combining the ASCA and EUVE results one can get better constraints on the temperature distribution, elemental abundances and hydrogen column density. In particular, it should be possible to derive the differential emission measure (DEM) distribution for the coronal plasma emitting in the EUVE and ASCA passbands, provided temporal variations between non-simultaneous observations do not play a major role. EUVE is very sensitive to the DEM distribution at temperatures less than a several million Kelvin, while ASCA is more sensitive to temperatures in excess of $\sim 10^7$ K. By combining the ASCA and EUVE data, we can determine the physical properties of the corona of λ And much better than with either ASCA or EUVE alone.

Acknowledgements. The authors acknowledge partial support from Ministero dell'Universitá e della Ricerca Scientifica e Tecnologica, the Italian Space Agency, and GNA-CNR. JJD was supported by the AXAF Science Center NASA contract NAS8-39073 during the course of this work.

References

Anders E., Grevesse N., 1989, Geochimica et Cosmochimica Acta 53, 157
Antunes A., Nagase F., White N.E., 1994, ApJ 436, L83
Arnaud M., Raymond J.C., 1992, ApJ 398, 394
Avni Y., 1976, ApJ 210, 642
Baliunas S.L., and Dupree A.K., 1979, ApJ 227, 870
Bocchino F., Maggio A., Sciortino S., 1994, ApJ 437, 209
Bauer F., Bregman J.N., 1996, ApJ 457, 382
Culhane J.L., White N.E., Shafer R.A., Parmar A.N., 1990, MNRAS 243, 424
Day C., Arnaud K., Ebisawa K., et al. 1995, *The ABC Guide to ASCA Data Reduction*, NASA/GSFC
Dempsey R.C., Linsky J.L., Fleming T.A., Schmitt J.H.M.M., 1993a, ApJS 86, 599
Dempsey R.C., Linsky J.L., Schmitt J.H.M.M., Fleming T.A., 1993b, ApJ 413, 333
Dotani T., et al. 1996, AscaNews no. 4
Drake S.A., Singh K.P., White N.E., Simon T., 1994, ApJ 436, L87
Drake J.J., Laming J.M., Widing K., 1995, ApJ 443, 393
Drake J.J., Laming J.M., Widing K., 1996a, In: S. Bowyer, R. Malina (eds.) Astrophysics in the EUV. Kluwer, Dordrecht, p. 97
Drake J.J., Laming J.M., Widing K., 1996b, ApJ, in press
Dupree A.K., Brickhouse N.S., Hanson G.J., 1996, In: S. Bowyer, R. Malina (eds.) Astrophysics in the EUV. Kluwer, Dordrecht, p. 141
Edvardsson B., Andersen J., Gustafsson B., et al. 1993, A&A 275, 101
Eker Z., 1992, ApJS 79, 481
Fekel F.C., Quigley R., Gillies K., Africano J.L., 1987, AJ 94, 726
Feldman U., 1992, Phys. Scripta 42, 202
Fiore F., Elvis M., McDowell J.C., Siemiginowska A., Wilkes B.J., 1994, ApJ 431, 515
Gehrels N., 1986, ApJ 303, 336
Giménez A., Reglero V., DeCastro E., Fernàndez-Figueroa M.J., 1991, A&A 248, 563
Gotthelf E.V., Jalota L., Mukai K., White N.E., 1994, ApJ 436, L91
Güedel M., Guinan E.F., Mewe R., Kaastra J.S., Skinner S.L., 1997, ApJ, in press
Habets G.M.H.J., Zwaan C., 1989, A&A 211, 56
Hall S.D., 1976, In: W.S. Fitch (ed.) Multiple Periodic Variable Stars. Reidel, Dordrecht, p. 287
Helfer H.L., Wallerstein G., 1968, ApJS 16, 1
Lallement R., Linsky J.F., Lequeux J., Baranov V.B., 1996, In: The Heliosphere in the Local Interstellar Medium, in press (Colorado Astrophysics Preprint # 302)
Majer P., Schmitt J.H.M.M., Golub L., Harnden F.R., Jr., Rosner R., 1986, ApJ 300, 360
Mewe R., Kaastra J.S., Liedhal D.A., 1995, *Legacy*, The Journal of the HEASARC, 6, 17
Mewe R., Kaastra J.S., Schrijver C.J., Van den Oord G.H.J., Alkemade F.J.M., 1995, A&A 296, 477
Mewe R., Kaastra J.S., White S.M., Pallavicini R., 1996, A&A 315, 170
Mewe R., Schrijver C.J., 1987, A&A 169, 178
Meyer J.-P., 1993, In: N. Pratzos, E. Vangioni-Flam, M. Cassé (eds.) Origin & Evolution of the Elements. CUP, p. 26
Morrison R., MacCammon D., 1983, ApJ 270, 119
Morale F., Micela G., Favata F., Sciortino S., 1996, A&AS 119, 403
Naftilan S.A., Drake S.A., 1977, ApJ 216, 508
Naftilan S.A., Drake S.A., 1980, PASP 92, 675
Olsen E.H., 1984, A&AS 57, 443
Ortolani A., Pallavicini R., Tagliaferri G., 1997, A&A, submitted
Pasquini L., Schmitt J.H.M.M., Pallavicini R., 1989, A&A 226, 225
Paresce F., 1984, AJ 89, 1022
Randich S., Gratton R., Pallavicini R., 1993, A&A 273, 194
Randich S., Giampapa M.S., Pallavicini R., 1994, A&A 283, 893
Raymond J.C., Smith B.W., 1977, ApJS 35, 419
Rumph T., Bowyer S., Vennes S., 1994, AJ 107, 2108
Savanov I.S., Berdyugina S.V., 1994, Pis'ma Astron. Zh. 20, 279
Schmitt J.H.M.M., Drake J.J., Stern R.A., 1996a, ApJ 465, L51
Schmitt J.H.M.M., Stern R.A., Drake J.J., Kürster M., 1996b, ApJ 464, 898
Schrijver C.J., van den Oord G.H.J., Mewe R., 1994, A&A 289, L23
Schrijver C.J., Mewe R., van den Oord G.H.J., Kaastra J.S., 1995, A&A 302, 438
Schrijver C.J., Zwaan C., 1991, A&A 251, 183
Singh K.P., Drake S.A., White N.E., 1995, ApJ 445, 840
Singh K.P., White N.E., Drake S.A., 1996, ApJ 456, 766
Snowden S.L., Turner T.J., George J.M., Yusaf R., 1995, OGIP Calibration Memo CAL/ROS/95-003
Stern R.A., Lemen J.R., Schmitt J.H.M.M., Pye J.P., 1995, ApJ 44, L45
Strassmeier K.G., Hall D.S., Boyd L.J., Genet R.M., 1989, ApJS 69, 141
Swank J.H., White N.E., Holt S.S., Becker R.H., 1981, ApJ 246, 208
Tanaka Y., Inoue H., Holt S.S., 1994, PASJ 46, L37
Tagliaferri G., Covino, S., Fleming T.A., et al. 1996, A&A, in press
Tautvaisiene G., Kriukelis S., Bikmaev I., 1992, Balt. Astron. 1, 450
Taylor B.J., 1991, ApJS 76, 715
White N.E., Shafer R.A., Horne K., Parmar A.N., Culhane J.L., 1990, ApJ 350, 776
White N.E., Arnaud K., Day C., et al. 1994, PASJ 46, L97
Wood B.E., Linsky J.L., 1996, ApJ, in press
Wood B.E., Alexander W.R., Linsky J.L., 1996, ApJ, in press

This article was processed by the author using Springer-Verlag LaTeX A&A style file *L-AA* version 3.